homogenates from the heart [9,10]. Excessive NE level and cardiac PNMT activity may provide the prerequisite for cardiac EPI synthesis evoked by ischemia. We speculate that ischemia may promote EPI synthesis and release by high NE accumulation via cardiac PNMT activity.

We have demonstrated the usefulness of dialysis technique for the in vivo monitoring of regional myocardial interstitial catecholamine kinetics [11,12]. In the present study, we extend this approach to assessment of PNMT activity using NE as a substrate of EPI synthesis. We examined the role of PNMT activity in the EPI release evoked by myocardial ischemia. Furthermore, we examined the contribution of neuronal catecholamine transport to EPI release evoked by ischemia.

2. Materials and methods

2.1. Animal preparation

Animal care proceeded in strict accordance with the *Guide for the Care and Use of Laboratory Animals* published by the US National Institute of Health (NIH Publication No. 85-23, revised 1996). Adult Japanese white rabbits (2.5–3.3 kg) were anesthetized with pentobarbital sodium (30–35 mg/kg i.v.). The level of anesthesia was maintained with a continuous intravenous infusion of pentobarbital sodium (1–2 mg/kg/h). The rabbits were intubated and ventilated with room air mixed with oxygen. Heart rate, arterial pressure, and electrocardiogram were simultaneously monitored with a data recorder. The fifth or sixth rib on the left side was partially removed to expose the heart. A snare was placed around the main branch of the left circumflex coronary artery (LCX) to act as the occluder for later coronary occlusion. With a fine guiding needle, a dialysis probe was implanted in the region perfused by LCX of the left ventricular wall. Judging from changes in the color of the ventricular wall during a brief coronary occlusion, the dialysis probe was located in the midst of the ischemic region. Heparin sodium (100 IU/kg) was administered intravenously to prevent blood coagulation.

2.2. Dialysis technique and epinephrine measurements

Materials suitable for cardiac dialysis probes have been described in detail elsewhere [13]. Briefly, we designed a handmade long transverse dialysis probe. A dialysis fiber (8 mm length, 0.31 mm o.d., and 0.20 mm i.d.; PAN-1200 50,000 molecular weight cutoff, Asahi Chemical Japan) was glued at both ends of a polyethylene tube. The dialysis probe was perfused with Ringer's solution or Ringer's solution containing pharmacological agents at a perfusion speed of 2 μl/min using a microinjection pump (Carnegie Medicine CMA/100). One sampling period was 15 min (1 sampling volume = 30 μl). Each sample was collected in a microtube containing 3 μl of 0.1 N HCl to prevent amine oxidation. Dialysate EPI and NE level were measured by high-performance liquid chromatography with electrochemical detection (ECD-300, Eicom, Kyoto, Japan) as previously described [14,15]. Dialysate EPI level served as an index of myocardial interstitial EPI level. We commenced the protocol followed by a stabilization period of 2 h. Taking into consideration the dead space between the dialysis fiber and sample tube, we sampled the dialysate.

2.3. Experimental protocols

2.3.1. Dialysate EPI levels during local administration of NE

First, to elucidate cardiac PNMT activity, we locally administered NE. The concentration of NE was chosen to be in the same range as in the myocardial ischemic region based on the results of our previous study [6]. After control sampling, we locally administered NE (250 or 2500 ng/ml) through a dialysis probe for 60 min, with dialysate collected during the last 15 min. The same protocol was followed after administration of a PNMT inhibitor (SKF29661) [16] in separate rabbits. SKF29661 (50 mg/kg) was administered intraperitoneally 60 min before control sampling. To confirm whether PNMT activity was located in sympathetic nerve endings or myocardium, we performed chemical sympathetic denervation with hydroxydopamine (6-OHDA) and examined the dialysate EPI response to local NE infusion. Five days previously, rabbits were given 60 mg/kg 6-OHDA intravenously [17]. Dialysate EPI response to NE infusion was measured. Furthermore, we examined the effect of NE uptake$_2$ inhibition on the EPI response to local NE infusion. We added corticosterone (1 mM) on the perfusate and measured the dialysate EPI response to local NE infusion.

2.3.2. Time course of dialysate EPI levels during the myocardial ischemia in the presence and absence of SKF29661

After control sampling, we occluded the main branch of LCX for 60 min and then released the occluder. We observed the time course of dialysate EPI levels in the ischemic region in six rabbits. We collected five consecutive 15-minute dialysate samples during coronary occlusion and reperfusion (vehicle group). To examine the involvement of PNMT activity on the EPI level, we intraperitoneally administered a PNMT inhibitor (SKF29661) 60 min before control sampling in separate rabbits (SKF group). We performed LCX occlusion and collected dialysate samples as described in vehicle group. We compared EPI responses to LCX occlusion between vehicle and SKF groups.

2.3.3. Influence of desipramine on dialysate EPI levels during myocardial ischemia with and without SKF29661

EPI can be released via non-exocytotic release at the sympathetic nerve terminals [18]. To elucidate the involvement of catecholamine transporter on EPI levels, we locally administered an inhibitor of NE uptake$_1$ carrier desipramine (100 μM) through a dialysis probe. One hour thereafter, we performed LCX occlusion and collected dialysate samples in

Table 1
Time course of heart rate and mean arterial pressure during coronary occlusion and reperfusion

	Control	Coronary occlusion (min)				Reperfusion (min)
		15	30	45	60	15
Heart rate (bpm)						
Vehicle group ($n=6$)*	297±10	289±8	283±9	280±9	281±7	269±6
SKF29661 group ($n=6$)	319±11	312±12	311±13	313±13	311±14	306±13
Desipramine group ($n=6$)	312±10	315±11	317±10	318±12	314±13	309±12
Desipramine+SKF29661 group ($n=6$)	316±12	310±10	314±8	315±7	317±8	311±8
Mean arterial pressure (mm Hg)						
Vehicle group ($n=6$)	96±8	87±7	84±5	83±4	81±5	81±3 †
SKF29661 group ($n=6$)	97±3	93±4	93±4	92±4	92±4	91±4 †
Desipramine group ($n=6$)	98±6	94±6	91±5	89±5	88±4	87±4 †
Desipramine+SKF29661 group ($n=6$)	101±2	88±6	90±4	88±4	88±3	83±3 †

†Values are means±SE. *$P<0.05$ vs. values of pretreatment groups.

the above-described protocol in separate rabbits (desipramine group). Furthermore, we tried to determine the influence of desipramine on PNMT induced EPI release during myocardial ischemia. We co-administered intraperitoneally SKF29661 (50 mg/kg) and desipramine locally through a dialysis probe continuously 60 min before control sampling (desipramine+SKF group). We performed LCX occlusion and collected dialysate samples as described in vehicle group. We compared EPI responses to LCX occlusion between desipramine and desipramine+SKF groups.

At the end of each experiment, the rabbits were killed with an overdose of pentobarbital sodium, and the implant regions were checked to confirm that the dialysis probe had been implanted within the cardiac muscle.

2.4. Statistical methods

The effects of myocardial ischemia (NE infusion) and pretreatment were examined using two-way analysis of variance. When statistical significance was detected between two groups, the dialysate EPI levels with and without a PNMT inhibitor were compared by unpaired *t*-test. The dialysate NE levels were compared among four groups using one-way analysis variance followed by Newman–Keuls test for the multiple comparisons against each other. The data of heart rate and mean arterial pressure were compared among four groups using two-way analysis variance. When statistical significance was detected, the Newman–Keuls test was applied. Statistical significance was defined as $P<0.05$. Values are presented as means±SE.

3. Results

3.1. Time course of heart rate and mean arterial pressure

Local administration of NE through a dialysis probe did not alter heart rate (HR) or mean arterial pressure (MAP) in vehicle or SKF groups. The time course of HR and MAP during myocardial ischemia and reperfusion is shown in Table 1. Coronary occlusion tended to cause a fall in HR and MAP, but no statistically significant alterations in HR or MAP were obtained against a baseline value within each group. Basal HR in vehicle group was lower than that in the other three groups.

3.2. Dialysate EPI response during local NE administration through a dialysis probe

Fig. 1 shows data obtained from local administration of exogenous NE through a dialysis probe. Dialysate EPI levels increased significantly with increases in the rate of NE infusion. Dialysate EPI levels reached 734.5±125, and 2081±367 pg/ml ($n=6$) at 250 and 2500 ng/ml of NE infusion, respectively. In the presence of SKF29661, dialysate EPI levels were significantly suppressed compared to those of the vehicle group. Dialysate EPI levels were 68±25, 282±70 pg/ml ($n=6$) at 250 and 2500 ng/ml of NE infusion, respectively. SKF29661 attenuated EPI responses to 10% of vehicle group. In sympathetic denervation with 6-OHDA, the dialysate EPI response to NE infusion (250 ng) was preserved ($n=4$, 760±193 pg/ml). With the perfusate containing the NE uptake$_2$ inhibitor, corticosterone (1 mM), the dialysate EPI response to NE infusion (250 ng) was suppressed ($n=6$, 167±27 pg/ml).

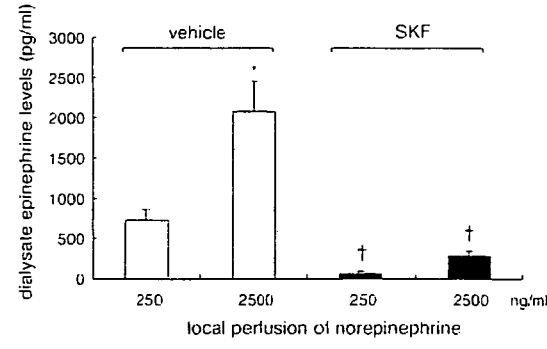

Fig. 1. Dialysate epinephrine levels evoked by norepinephrine perfusion through dialysis probe. SKF = SKF29661. *$P<0.05$ vs. value at 0–15 min of norepinephrine perfusion. †$P<0.05$ vs. concurrent value of vehicle group.

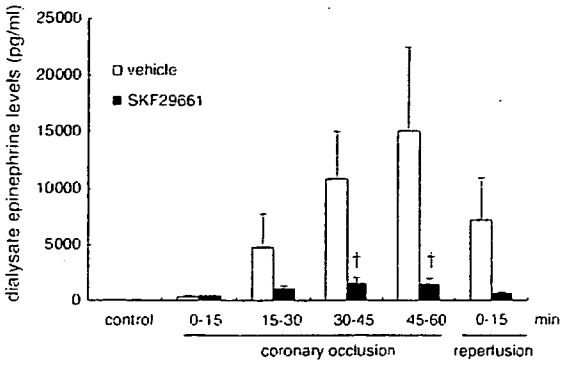

Fig. 2. Time course of dialysate epinephrine levels during coronary occlusion. Values are means±SE. †$P<0.05$ vs. concurrent value of vehicle group.

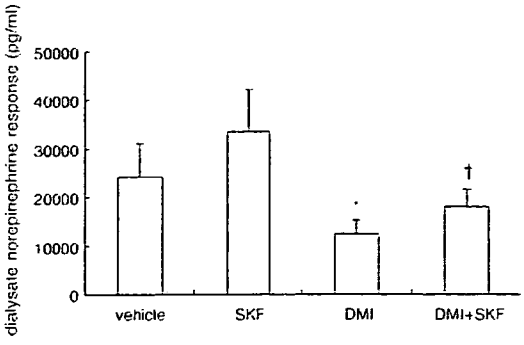

Fig. 4. Dialysate norepinephrine responses to 60 min coronary occlusion. SKF = SKF29661, DMI = desipramine, DMI+SKF = desipramine+SKF29661. Values are means±SE. *$P<0.05$ vs. value of vehicle group. †$P<0.05$ vs. value of SKF group.

3.3. Dialysate EPI levels in the ischemic region

Coronary occlusion significantly increased dialysate EPI levels (Fig. 2). In the vehicle group, dialysate EPI levels were 59.6±39.8 pg/ml in the control and increased after coronary occlusion. During 60 min coronary occlusion, dialysate EPI levels markedly increased and reached 15030±7418 pg/ml ($n=6$) at 45–60 min of occlusion. After reperfusion, dialysate EPI levels decreased to 7193±3722 pg/ml, although their levels were higher than those in the control. In the presence of SKF29661, dialysate EPI levels also increased and reached 1493±196 pg/ml ($n=6$) at 45–60 min of occlusion. These increases in dialysate EPI levels after 30 min of coronary occlusion were significantly attenuated by SKF29661.

3.4. Dialysate EPI levels in the ischemic region during local desipramine administration

Although coronary occlusion increased dialysate EPI levels, these levels were suppressed during local desipramine administration compared to the vehicle group (Fig. 3). During 60 min coronary occlusion, dialysate EPI levels increased and reached 743±171 pg/ml ($n=6$) at 45–60 min of occlusion. After reperfusion, dialysate EPI levels decreased to 400±181 pg/ml, although their levels were higher than those in the control. In the presence of SKF29661, dialysate EPI levels also increased and reached 725±154 pg/ml ($n=6$) at 45–60 min of occlusion. These increases in dialysate EPI levels were not attenuated by SKF29661.

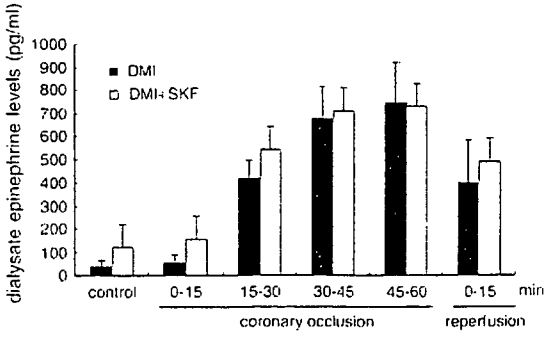

Fig. 3. Influence of desipramine on dialysate EPI levels during myocardial ischemia with and without SKF29661. DMI = desipramine, DMI+SKF = desipramine+SKF29661. Values are means±SE.

3.5. Comparison of peak dialysate NE levels of the 4 groups

EPI is synthesized from NE, and so myocardial interstitial NE levels might affect myocardial interstitial EPI levels. We compared with myocardial interstitial NE levels at 45–60 min of coronary occlusion in the vehicle group, the SKF29661 group, the desipramine group and the desipramine and SKF29661 group (Fig. 4) ($n=6$-6-6-6). In the latter two groups (desipramine, desipramine+SKF29661), ischemia-induced peak dialysate NE levels were significantly suppressed in comparison with that of the vehicle or SKF29661 group. Calculated ratios of interstitial EPI/NE were 1.5±0.4 and 12±4% at NE infusion (250 ng) and 45–60 min of occlusion, respectively.

4. Discussion

4.1. Changes in myocardial interstitial EPI levels during local administration of NE through a dialysis probe

Local administration of NE dose dependently increased dialysate EPI levels. The pretreatment with PNMT inhibitor SKF29661 significantly suppressed these increases. Therefore, the EPI levels in dialysate could serve as an index of PNMT activity during local administration of NE. To our knowledge, this is the first direct assessment of cardiac PNMT activity in in vivo heart. These results indicate that EPI can be regionally synthesized from NE with PNMT activity in the heart. Regionally administered NE in myocardial interstitium was taken up by cardiac sympathetic nerve endings via the uptake$_1$ carrier or by extraneuronal cells via uptake$_2$ carrier [19–21]. Several studies demonstrated the existence of PNMT in the myocardium rather than

sympathetic nerve endings [17,22]. In sympathetic denervation with 6-OHDA, the dialysate EPI response to NE infusion was preserved. The dialysate EPI response was suppressed by pretreatment with corticosterone (an NE $uptake_2$ inhibitor). Our data were also consistent with those studies. NE might be taken up by myocardial cell via $uptake_2$ carrier and converted to EPI with PNMT. Recent study has shown that gene expression of the PNMT is localized not in cardiac ganglion, but in cardiomyocytes [23]. Therefore, our data suggest that high NE level in myocardial interstitium yields EPI synthesis by regional PNMT activity. NE that was taken up by extraneuronal cells was metabolized mainly to normetanephrine (NMN) or 3-methoxy-4-hydroxyphenylglycol (MHPG) by catechol *O*-methyltransferase (COMT) [19], but high NE was partly available for EPI synthesis with PNMT. These elevated NE levels were similar to the levels of myocardial ischemic regions in our previous studies [6,24]. Therefore, EPI synthesis with PNMT may gain relevance during myocardial ischemia.

4.2. Myocardial interstitial EPI levels during coronary artery occlusion

Coronary occlusion-induced progressive increases in dialysate EPI levels. These increases corresponded to increases in dialysate NE levels. Our data suggest that the high NE level evoked by myocardial ischemia yields EPI synthesis by regional PNMT activity. During myocardial ischemia, calculated ratio of interstitial EPI/NE was eight-times higher than that of NE infusion. In the ischemic heart, normal transport of NE is impaired because of a reduced sodium gradient [5], whereas another uptake system is operative by extraneuronal cells via the $uptake_2$ carrier which is independent of the sodium gradient [25]. Actually myocardial ischemia evoked increases in myocardial interstitial NMN or MHPG via the $uptake_2$ carrier [26]. The time course of dialysate EPI levels corresponded to increases in dialysate NE and NMN levels. Therefore, we consider that released NE is taken up by extraneuronal cells and PNMT activity for EPI synthesis is operative at high concentration of NE.

To confirm EPI synthesis via PNMT activity, we examined ischemia-induced dialysate EPI levels in the presence and absence of a PNMT inhibitor. PNMT inhibition suppressed the increase in dialysate EPI (synthesis by PNMT) and augmented the increase in dialysate NE (substrate of PNMT) levels. Thus, in the ischemic period as well as local administration of NE, PNMT activity plays an important physiological role in NE gradation and EPI synthesis. The PNMT activity in the ischemic left ventricle augmented EPI production by excess of substrate. The increased PNMT activity might reflect compensatory or adaptation processes secondary to impairments of the catecholamine uptake system and its degradation via monoamine oxidase [6].

At the myocardial interstitial space, local ω-conotoxin GVIA treatment attenuated the EPI release in response to cardiac sympathetic nerve stimulation [18]. Furthermore, local tyramine administration caused an increase in dialysate EPI level via a non-exocytotic mechanism. The previous study demonstrated that EPI is released from vesicle and axoplasma via exocytosis and carrier-mediated transport in the cardiac sympathetic nerve endings. In the resting state, myocardial interstitial EPI is extracted mainly from circulating EPI and taken up via catecholamine transporter to nerve endings. Therefore, in the sympathetic nerve endings containing EPI, the non-exocytotic release via outward transport would be involved in EPI release evoked by myocardial ischemia.

Myocardial ischemia-induced increases in dialysate EPI levels were suppressed by the pretreatment with desipramine. Desipramine suppressed peak EPI levels by 5% of vehicle group. Marked suppression of EPI release can be explained by two possible mechanisms. First, desipramine inhibits both directions of NE transport through $uptake_1$ carrier [5,27]. Ischemia-induced outward NE transport through $uptake_1$ carrier is inhibited by desipramine, and so myocardial interstitial NE levels are also attenuated [6]. In this way, desipramine reduced the substrate of EPI via PNMT and EPI synthesis in extraneuronal cells. Alternatively, EPI is released via carrier-mediated outward transport of EPI from sympathetic nerve endings. The present study could not clarify whether EPI specific transporter or NE transporter is involved in carrier-mediated outward transport of EPI. But desipramine inhibits transports of both EPI and NE. Thus, both actions of desipramine on NE and EPI caused a marked decrease in the EPI release evoked by myocardial ischemia. Although desipramine markedly suppressed the EPI release evoked by myocardial ischemia, it is uncertain which factor is more responsible for EPI release.

Finally, to elucidate which of these two mechanisms is mainly involved in the EPI release evoked by myocardial ischemia, we compared ischemia-induced EPI release between desipramine alone and the combination of desipramine and SKF29661 pretreatments. Myocardial ischemia-induced EPI release did not differ between the two groups. This result indicates that the EPI synthesis by PNMT might not be involved in the EPI release evoked by myocardial ischemia. In the presence of desipramine, myocardial interstitial NE levels were markedly suppressed. These NE levels might not be operative as the substrate of EPI whereas only the markedly higher NE level in vehicle group might be operative as the substrate of EPI and yield EPI synthesis via PNMT activity. Thus, PNMT in the left ventricle is capable of synthesizing EPI with markedly elevated NE in the myocardial interstitial space. As well as COMT system [28], cardiac PNMT plays an important physiological role in NE degradation during high concentrations of myocardial interstitial NE. Since EPI preferentially interacts with $beta_2$-adrenergic receptors in heart [29]. Regional EPI might promote exocytotic NE release by activating presynaptic $beta_2$-adrenergic receptors. Future work should concentrate on these aspects of cardiac PNMT.

4.3. Methodological considerations

In general, EPI is released from the adrenal medulla and carried to the heart via the bloodstream [9]. In the present study, we administered a PNMT inhibitor SKF29661 intraperitoneally to block EPI synthesis. SKF29661 may inhibit EPI synthesis at the adrenal grand and reduce blood EPI levels. In this way, administration of SKF29661 might affect EPI uptake and the content of EPI at the cardiac sympathetic nerve endings. There was no significant difference in the control dialysate EPI level between vehicle and SKF29661 group. Therefore, we believe that extraction of EPI from plasma EPI does not change the quantitative results obtained from the cardiac dialysis.

Animal studies demonstrated that two enzymes are involved in EPI synthesis: PNMT and nonspecific *N*-methyltransferase [30]. Nonspecific *N*-methyltransferase is less inhibited by the PNMT inhibitor SKF29661. This nonspecific *N*-methyltransferase was reported to be present in the heart, but the predominant cardiac enzyme is apparently PNMT. Actually pretreatment with SKF29661 suppressed NE-induced EPI release by 10% of vehicle group. Therefore, it is thought that nonspecific *N*-methyltransferase exerts little effect on the EPI release evoked by NE administration or myocardial ischemia.

In conclusion, there is a PNMT activity in the heart. Under local administration of NE or ischemic conditions, PNMT in the left ventricle is capable of synthesizing EPI with markedly elevated NE in the myocardial interstitial space. We consider two mechanisms to be involved in the increment of EPI during myocardial ischemia, namely EPI synthesis by cardiac PNMT in extraneuronal cells and the non-exocytotic release from the sympathetic nerve endings.

Acknowledgements

This work was supported by Grants-in-Aid for scientific research (17591659) from the Ministry of Education, Culture, Sports, Science and Technology. The authors thank Glaxosmithkline for the supply of SKF29661.

References

[1] Lameris TW, de Zeeuw S, Alberts G, Boomsma F, Duncker DJ, Verdouw PD, et al. Time course and mechanism of myocardial catecholamine release during transient ischemia in vivo. Circulation 2000;101:2645–50.

[2] Kuroko Y, Fujii T, Yamazaki T, Akiyama T, Ishino K, Sano S, et al. Contribution of catechol *O*-methyltransferase to the removal of accumulated interstitial catecholamines evoked by myocardial ischemia. Neurosci Lett 2005;388:61–4.

[3] Penny WJ. The deleterious effects of myocardial catecholamines on cellular electrophysiology and arrhythmias during ischaemia and reperfusion. Eur Heart J 1984;5:960–73.

[4] Waldenstrom AP, Hjalmarson AC, Thornell L. A possible role of noradrenaline in the development of myocardial infarction: an experimental study in the isolated rat heart. Am Heart J 1978;95: 43–51.

[5] Schömig A, Dart AM, Dietz R, Mayer E, Kubler W. Release of endogenous catecholamines in the ischemic myocardium of the rat. Part A: locally mediated release. Circ Res 1984;55:689–701.

[6] Akiyama T, Yamazaki T. Myocardial interstitial norepinephrine and dihydroxyphenylglycol levels during ischemia and reperfusion. Cardiovasc Res 2001;49:78–85.

[7] Axelrod J. Purification and properties of phenylethanolamine-*N*-methyl transferase. J Biol Chem 1962;237:1657–60.

[8] Peronnet F, Boudreau G, de Champlain J, Nadeau R. Effect of changes in myocardial epinephrine stores on plasma norepinephrine gradient across the dog heart. Am J Physiol 1994;266:H2404–9.

[9] Elayan HH, Kennedy BP, Ziegler MG. Cardiac atria and ventricles contain different inducible adrenaline synthesising enzymes. Cardiovasc Res 1990;24:53–6.

[10] Ziegler MG, Bao X, Kennedy BP, Joyner A, Enns R. Location, development, control, and function of extraadrenal phenylethanolamine *N*-methyltransferase. Ann N Y Acad Sci 2002;971:76–82.

[11] Akiyama T, Yamazaki T, Ninomiya I. Differential regional responses of myocardial interstitial noradrenaline levels to coronary occlusion. Cardiovasc Res 1993;27:817–22.

[12] Yamazaki T, Akiyama T, Kitagawa H, Takauchi Y, Kawada T, Sunagawa K. A new, concise dialysis approach to assessment of cardiac sympathetic nerve terminal abnormalities. Am J Physiol 1997;272:H1182–7.

[13] Akiyama T, Yamazaki T, Ninomiya I. In vivo monitoring of myocardial interstitial norepinephrine by dialysis technique. Am J Physiol 1991;261: H1643–7.

[14] Yamazaki T, Akiyama T, Shindo T. Routine high-performance liquid chromatographic determination of myocardial interstitial norepinephrine. J Chromatogr B Biomed Appl 1995;670:328–31.

[15] Takauchi Y, Kitagawa H, Kawada T, Akiyama T, Yamazaki T. High-performance liquid chromatographic determination of myocardial interstitial dihydroxyphenylglycol. J Chromatogr B Biomed Sci Appl 1997;693:218–21.

[16] Kennedy B, Elayan H, Ziegler MG. Lung epinephrine synthesis. Am J Physiol 1990;258:L227–31.

[17] Tse J, Rodriques E, Gonzalez M, Weiss HR. Effects of chemical denervation with 6-hydroxydopamine on myocardial responsiveness to isoproterenol in rabbits. Basic Res Cardiol 1995;90:380–7.

[18] Kawada T, Yamazaki T, Akiyama T. Local epinephrine release in the rabbit myocardial interstitium in vivo. J Auton Nerv Syst 2000;78: 94–8.

[19] Trendelenburg U. The extraneuronal uptake and metabolism of catecholamines in the heart. In: Paton DM, editor. The mechanism of neuronal and extraneuronal transport of catecholamines. 1st ed. New York: Raven Press; 1976. p. 259–80.

[20] Grohmann M, Trendelenburg U. The substrate specificity of uptake$_2$ in the rat heart. Naunyn Schmiedebergs Arch Pharmacol 1984;328: 164–73.

[21] Obst OO, Rose H, Kammermeier H. Characterization of catecholamine uptake$_2$ in isolated cardiac myocytes. Mol Cell Biochem 1996;163–164: 181–3.

[22] Torda T, Culman J, Petrikova M. Distribution of phenylethanolamine-*N*-methytransferase in the rat heart: effect of 6-hydroxydopamine. Eur J Pharmacol 1987;141:305–8.

[23] Krizanova O, Micutkova L, Jelokova J, Filipenko M, Sabban E, Kvetnansky R. Existence of cardiac PNMT m-RNA in adult rats: elevation by stress in a glucocorticoid-dependent manner. Am J Physiol Heart Circ Physiol 2001;281:H1372–9.

[24] Shindo T, Akiyama T, Yamazaki T, Ninomiya I. Regional myocardial interstitial norepinephrine kinetics during coronary occlusion and reperfusion. Am J Physiol 1996;270:H245–51.

[25] Schömig E, Russ H, Staudt K, Martel F, Gliese M, Gründemann. The extraneuronal monoamine transporter exists in human central nervous system glia. Adv Pharmacol 1998;42:356–9.

[26] Fujii T, Yamazaki T, Akiyama T, Sano S, Mori H. Extra neuronal enzymatic degradation of myocardial norepinephrine in the ischemic region. Cardiovasc Res 2004;64:125–31.

[27] Schömig A, Fischer S, Kurz T, Richardt G, Schomig E. Nonexocytotic release of endogenous noradrenaline in during in the ischemic and anoxic rat heart: mechanism and metabolic requirements. Circ Res 1987;60:194–205.
[28] Carlsson L, Graefe KH, Trendelenburg U. Early intraneuronal mobilization and deamination of noradrenaline during global ischemia in the isolated perfused rat heart. Naunyn Schmiedebergs Arch Pharmacol 1987;336:508–18.
[29] Lands AM, Arnold A, McAuliff JP, Luduena FP, Brown Jr TG. Differentiation of receptor systems activated by sympathmimetic amines. Nature 1967;214:597–8.
[30] Zeigler MG, Kennedy B, Elayan H. Extraadrenal adrenaline formation by two separate enzymes. Experintia 1989;45:718–20.

ELSEVIER

Cardiovascular Research 74 (2007) 438–444

Cardiovascular Research

www.elsevier.com/locate/cardiores

Cardiac epinephrine synthesis and ischemia-induced myocardial epinephrine release

Yosuke Kuroko [a], Toji Yamazaki [b,*], Noriyuki Tokunaga [a], Tsuyoshi Akiyama [b], Hirotoshi Kitagawa [b], Kozo Ishino [a], Shunji Sano [a], Hidezo Mori [b]

[a] *Department of Cardiovascular Surgery, Okayama University Graduate School of Medicine and Dentistry, Okayama, 700-8558, Japan*
[b] *Department of Cardiac Physiology, National Cardiovascular Center Research Institute, 5-7-1 Fujishiro-dai, Suita, Osaka, 565-8565, Japan*

Received 4 September 2006; received in revised form 13 February 2007; accepted 14 February 2007
Available online 21 February 2007
Time for primary review 15 days

Abstract

Objective: Phenylethanolamine-*N*-methyltransferase (PNMT), the enzyme that synthesizes epinephrine (EPI) from norepinephrine (NE) in the adrenal gland, is present in extra-adrenal tissues including heart. Ischemia evokes an excessive NE accumulation in the myocardial interstitial spaces. Therefore, cardiac PNMT activity with high NE levels may contribute to cardiac EPI synthesis and release evoked by ischemia.
Methods: We measured dialysate EPI levels in the left ventricle of anesthetized rabbits using a cardiac microdialysis technique. The dialysate EPI level served as an index of the myocardial interstitial EPI level. Locally administered NE-induced dialysate EPI responses were measured. The left circumflex coronary artery was occluded for 60 min and the dialysate EPI and NE levels in the ischemic region were measured. Coronary occlusion-induced EPI responses were compared with and without administration of a PNMT inhibitor (SKF29661) in the presence and absence of desipramine (catecholamine transport blocker).
Results: Local administration of NE (250, 2500 ng/ml) increased the EPI levels to 734 ± 125 and 2088 ± 367 pg/ml respectively. These increases in dialysate EPI were suppressed by the PNMT inhibitor. Acute myocardial ischemia significantly increased the EPI levels to 3607 ± 1069 pg/ml in the ischemic region, and these were suppressed by the PNMT inhibitor (1417 ± 581 pg/ml). The pretreatment with desipramine suppressed ischemia-induced EPI release, which did not differ with (725 ± 155 pg/ml) and without administration of a PNMT inhibitor (743 ± 172 pg/ml).
Conclusion: The cardiac PNMT in the left ventricle is capable of synthesizing EPI with markedly elevated NE levels in the myocardial interstitial space.

Keywords: Autonomic nervous system; Interstitial space; Ischemia; Reperfusion; Neurotransmitters

1. Introduction

It is generally accepted that myocardial ischemia evokes an excessive catecholamine accumulation in the myocardial interstitial space [1,2]. This high catecholamine level in the myocardial interstitium is thought to aggravate the progression of myocardial cell injury and incidence of malignant arrhythmia [3,4]. From in vitro and in vivo studies, several mechanisms are presently suggested to induce release of norepinephrine (NE) from the nerve endings [1,5,6]. The outward NE transport through uptake$_1$ carrier has been proposed as an important mechanism responsible for the ischemia-induced NE release. With respect to epinephrine (EPI), however, it is uncertain whether the mechanism of release differs between EPI and NE.

EPI is synthesized mainly from NE in the adrenal medulla by phenylethanolamine *N*-methyltransferase (PNMT) [7] and released into the bloodstream [8]. Myocardial ischemia evokes an excessive NE and EPI accumulation in the myocardial interstitial space although the blood supply is blocked. Therefore, regional release mechanism has been suggested to induce release of EPI in the ischemic region. Early studies reported that PNMT activity was measured in

* Corresponding author. Tel.: +81 6 6833 5012x2379; fax: +81 6 6872 8092.
E-mail address: yamazaki@ri.ncvc.go.jp (T. Yamazaki).

0008-6363/$ - see front matter © 2007 European Society of Cardiology. Published by Elsevier B.V. All rights reserved.
doi:10.1016/j.cardiores.2007.02.018

homogenates from the heart [9,10]. Excessive NE level and cardiac PNMT activity may provide the prerequisite for cardiac EPI synthesis evoked by ischemia. We speculate that ischemia may promote EPI synthesis and release by high NE accumulation via cardiac PNMT activity.

We have demonstrated the usefulness of dialysis technique for the in vivo monitoring of regional myocardial interstitial catecholamine kinetics [11,12]. In the present study, we extend this approach to assessment of PNMT activity using NE as a substrate of EPI synthesis. We examined the role of PNMT activity in the EPI release evoked by myocardial ischemia. Furthermore, we examined the contribution of neuronal catecholamine transport to EPI release evoked by ischemia.

2. Materials and methods

2.1. Animal preparation

Animal care proceeded in strict accordance with the *Guide for the Care and Use of Laboratory Animals* published by the US National Institute of Health (NIH Publication No. 85-23, revised 1996). Adult Japanese white rabbits (2.5–3.3 kg) were anesthetized with pentobarbital sodium (30–35 mg/kg i.v.). The level of anesthesia was maintained with a continuous intravenous infusion of pentobarbital sodium (1–2 mg/kg/h). The rabbits were intubated and ventilated with room air mixed with oxygen. Heart rate, arterial pressure, and electrocardiogram were simultaneously monitored with a data recorder. The fifth or sixth rib on the left side was partially removed to expose the heart. A snare was placed around the main branch of the left circumflex coronary artery (LCX) to act as the occluder for later coronary occlusion. With a fine guiding needle, a dialysis probe was implanted in the region perfused by LCX of the left ventricular wall. Judging from changes in the color of the ventricular wall during a brief coronary occlusion, the dialysis probe was located in the midst of the ischemic region. Heparin sodium (100 IU/kg) was administered intravenously to prevent blood coagulation.

2.2. Dialysis technique and epinephrine measurements

Materials suitable for cardiac dialysis probes have been described in detail elsewhere [13]. Briefly, we designed a handmade long transverse dialysis probe. A dialysis fiber (8 mm length, 0.31 mm o.d., and 0.20 mm i.d.; PAN-1200 50,000 molecular weight cutoff, Asahi Chemical Japan) was glued at both ends of a polyethylene tube. The dialysis probe was perfused with Ringer's solution or Ringer's solution containing pharmacological agents at a perfusion speed of 2 μl/min using a microinjection pump (Carnegie Medicine CMA/100). One sampling period was 15 min (1 sampling volume = 30 μl). Each sample was collected in a microtube containing 3 μl of 0.1 N HCl to prevent amine oxidation. Dialysate EPI and NE level were measured by high-performance liquid chromatography with electrochemical detection (ECD-300, Eicom, Kyoto, Japan) as previously described [14,15]. Dialysate EPI level served as an index of myocardial interstitial EPI level. We commenced the protocol followed by a stabilization period of 2 h. Taking into consideration the dead space between the dialysis fiber and sample tube, we sampled the dialysate.

2.3. Experimental protocols

2.3.1. Dialysate EPI levels during local administration of NE

First, to elucidate cardiac PNMT activity, we locally administered NE. The concentration of NE was chosen to be in the same range as in the myocardial ischemic region based on the results of our previous study [6]. After control sampling, we locally administered NE (250 or 2500 ng/ml) through a dialysis probe for 60 min, with dialysate collected during the last 15 min. The same protocol was followed after administration of a PNMT inhibitor (SKF29661) [16] in separate rabbits. SKF29661 (50 mg/kg) was administered intraperitoneally 60 min before control sampling. To confirm whether PNMT activity was located in sympathetic nerve endings or myocardium, we performed chemical sympathetic denervation with hydroxydopamine (6-OHDA) and examined the dialysate EPI response to local NE infusion. Five days previously, rabbits were given 60 mg/kg 6-OHDA intravenously [17]. Dialysate EPI response to NE infusion was measured. Furthermore, we examined the effect of NE uptake$_2$ inhibition on the EPI response to local NE infusion. We added corticosterone (1 mM) on the perfusate and measured the dialysate EPI response to local NE infusion.

2.3.2. Time course of dialysate EPI levels during the myocardial ischemia in the presence and absence of SKF29661

After control sampling, we occluded the main branch of LCX for 60 min and then released the occluder. We observed the time course of dialysate EPI levels in the ischemic region in six rabbits. We collected five consecutive 15-minute dialysate samples during coronary occlusion and reperfusion (vehicle group). To examine the involvement of PNMT activity on the EPI level, we intraperitoneally administered a PNMT inhibitor (SKF29661) 60 min before control sampling in separate rabbits (SKF group). We performed LCX occlusion and collected dialysate samples as described in vehicle group. We compared EPI responses to LCX occlusion between vehicle and SKF groups.

2.3.3. Influence of desipramine on dialysate EPI levels during myocardial ischemia with and without SKF29661

EPI can be released via non-exocytotic release at the sympathetic nerve terminals [18]. To elucidate the involvement of catecholamine transporter on EPI levels, we locally administered an inhibitor of NE uptake$_1$ carrier desipramine (100 μM) through a dialysis probe. One hour thereafter, we performed LCX occlusion and collected dialysate samples in

Table 1
Time course of heart rate and mean arterial pressure during coronary occlusion and reperfusion

	Control	Coronary occlusion (min)				Reperfusion (min)
		15	30	45	60	15
Heart rate (bpm)						
Vehicle group ($n=6$)*	297±10	289±8	283±9	280±9	281±7	269±6
SKF29661 group ($n=6$)	319±11	312±12	311±13	313±13	311±14	306±13
Desipramine group ($n=6$)	312±10	315±11	317±10	318±12	314±13	309±12
Desipramine+SKF29661 group ($n=6$)	316±12	310±10	314±8	315±7	317±8	311±8
Mean arterial pressure (mm Hg)						
Vehicle group ($n=6$)	96±8	87±7	84±5	83±4	81±5	81±3 †
SKF29661 group ($n=6$)	97±3	93±4	93±4	92±4	92±4	91±4 †
Desipramine group ($n=6$)	98±6	94±6	91±5	89±5	88±4	87±4 †
Desipramine+SKF29661 group ($n=6$)	101±2	88±6	90±4	88±4	88±3	83±3 †

†Values are means±SE. *$P<0.05$ vs. values of pretreatment groups.

the above-described protocol in separate rabbits (desipramine group). Furthermore, we tried to determine the influence of desipramine on PNMT induced EPI release during myocardial ischemia. We co-administered intraperitoneally SKF29661 (50 mg/kg) and desipramine locally through a dialysis probe continuously 60 min before control sampling (desipramine+SKF group). We performed LCX occlusion and collected dialysate samples as described in vehicle group. We compared EPI responses to LCX occlusion between desipramine and desipramine+SKF groups.

At the end of each experiment, the rabbits were killed with an overdose of pentobarbital sodium, and the implant regions were checked to confirm that the dialysis probe had been implanted within the cardiac muscle.

2.4. Statistical methods

The effects of myocardial ischemia (NE infusion) and pretreatment were examined using two-way analysis of variance. When statistical significance was detected between two groups, the dialysate EPI levels with and without a PNMT inhibitor were compared by unpaired *t*-test. The dialysate NE levels were compared among four groups using one-way analysis variance followed by Newman–Keuls test for the multiple comparisons against each other. The data of heart rate and mean arterial pressure were compared among four groups using two-way analysis variance. When statistical significance was detected, the Newman–Keuls test was applied. Statistical significance was defined as $P<0.05$. Values are presented as means±SE.

3. Results

3.1. Time course of heart rate and mean arterial pressure

Local administration of NE through a dialysis probe did not alter heart rate (HR) or mean arterial pressure (MAP) in vehicle or SKF groups. The time course of HR and MAP during myocardial ischemia and reperfusion is shown in Table 1. Coronary occlusion tended to cause a fall in HR and MAP, but no statistically significant alterations in HR or MAP were obtained against a baseline value within each group. Basal HR in vehicle group was lower than that in the other three groups.

3.2. Dialysate EPI response during local NE administration through a dialysis probe

Fig. 1 shows data obtained from local administration of exogenous NE through a dialysis probe. Dialysate EPI levels increased significantly with increases in the rate of NE infusion. Dialysate EPI levels reached 734.5±125, and 2081±367 pg/ml ($n=6$) at 250 and 2500 ng/ml of NE infusion, respectively. In the presence of SKF29661, dialysate EPI levels were significantly suppressed compared to those of the vehicle group. Dialysate EPI levels were 68±25, 282±70 pg/ml ($n=6$) at 250 and 2500 ng/ml of NE infusion, respectively. SKF29661 attenuated EPI responses to 10% of vehicle group. In sympathetic denervation with 6-OHDA, the dialysate EPI response to NE infusion (250 ng) was preserved ($n=4$, 760±193 pg/ml). With the perfusate containing the NE uptake$_2$ inhibitor, corticosterone (1 mM), the dialysate EPI response to NE infusion (250 ng) was suppressed ($n=6$, 167±27 pg/ml).

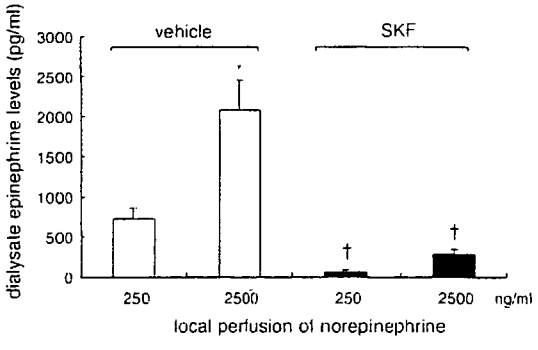

Fig. 1. Dialysate epinephrine levels evoked by norepinephrine perfusion through dialysis probe. SKF = SKF29661, *$P<0.05$ vs. value at 0–15 min of norepinephrine perfusion, †$P<0.05$ vs. concurrent value of vehicle group.

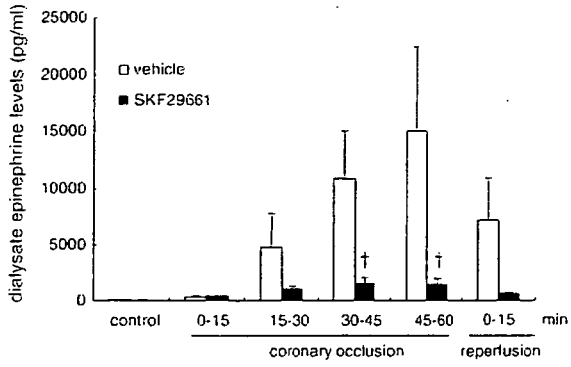

Fig. 2. Time course of dialysate epinephrine levels during coronary occlusion. Values are means±SE. †$P<0.05$ vs. concurrent value of vehicle group.

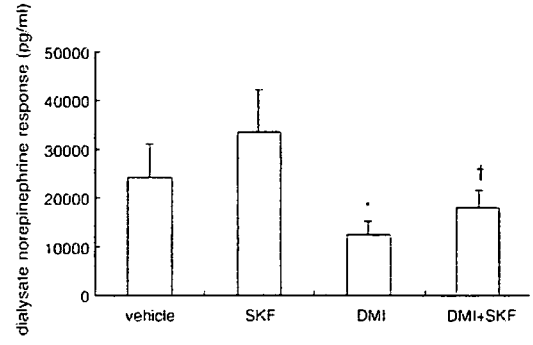

Fig. 4. Dialysate norepinephrine responses to 60 min coronary occlusion. SKF = SKF29661, DMI = desipramine, DMI+SKF=desipramine+SKF29661.Values are means±SE. *$P<0.05$ vs. value of vehicle group. †$P<0.05$ vs. value of SKF group.

3.3. Dialysate EPI levels in the ischemic region

Coronary occlusion significantly increased dialysate EPI levels (Fig. 2). In the vehicle group, dialysate EPI levels were 59.6±39.8 pg/ml in the control and increased after coronary occlusion. During 60 min coronary occlusion, dialysate EPI levels markedly increased and reached 15030±7418 pg/ml ($n=6$) at 45–60 min of occlusion. After reperfusion, dialysate EPI levels decreased to 7193±3722 pg/ml, although their levels were higher than those in the control. In the presence of SKF29661, dialysate EPI levels also increased and reached 1493±196 pg/ml ($n=6$) at 45–60 min of occlusion. These increases in dialysate EPI levels after 30 min of coronary occlusion were significantly attenuated by SKF29661.

3.4. Dialysate EPI levels in the ischemic region during local desipramine administration

Although coronary occlusion increased dialysate EPI levels, these levels were suppressed during local desipramine administration compared to the vehicle group (Fig. 3). During 60 min coronary occlusion, dialysate EPI levels increased and reached 743±171 pg/ml ($n=6$) at 45–60 min of occlusion. After reperfusion, dialysate EPI levels decreased to 400±181 pg/ml, although their levels were higher than those in the control. In the presence of SKF29661, dialysate EPI levels also increased and reached 725±154 pg/ml ($n=6$) at 45–60 min of occlusion. These increases in dialysate EPI levels were not attenuated by SKF29661.

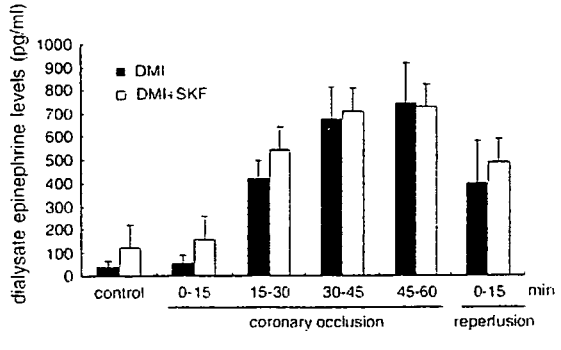

Fig. 3. Influence of desipramine on dialysate EPI levels during myocardial ischemia with and without SKF29661. DMI = desipramine, DMI+SKF = desipramine+SKF29661. Values are means±SE.

3.5. Comparison of peak dialysate NE levels of the 4 groups

EPI is synthesized from NE, and so myocardial interstitial NE levels might affect myocardial interstitial EPI levels. We compared with myocardial interstitial NE levels at 45–60 min of coronary occlusion in the vehicle group, the SKF29661 group, the desipramine group and the desipramine and SKF29661 group (Fig. 4) ($n=6$-6-6-6). In the latter two groups (desipramine, desipramine+SKF29661), ischemia-induced peak dialysate NE levels were significantly suppressed in comparison with that of the vehicle or SKF29661 group. Calculated ratios of interstitial EPI/NE were 1.5±0.4 and 12±4% at NE infusion (250 ng) and 45–60 min of occlusion, respectively.

4. Discussion

4.1. Changes in myocardial interstitial EPI levels during local administration of NE through a dialysis probe

Local administration of NE dose dependently increased dialysate EPI levels. The pretreatment with PNMT inhibitor SKF29661 significantly suppressed these increases. Therefore, the EPI levels in dialysate could serve as an index of PNMT activity during local administration of NE. To our knowledge, this is the first direct assessment of cardiac PNMT activity in in vivo heart. These results indicate that EPI can be regionally synthesized from NE with PNMT activity in the heart. Regionally administered NE in myocardial interstitium was taken up by cardiac sympathetic nerve endings via the uptake$_1$ carrier or by extraneuronal cells via uptake$_2$ carrier [19–21]. Several studies demonstrated the existence of PNMT in the myocardium rather than

sympathetic nerve endings [17,22]. In sympathetic denervation with 6-OHDA, the dialysate EPI response to NE infusion was preserved. The dialysate EPI response was suppressed by pretreatment with corticosterone (an NE uptake$_2$ inhibitor). Our data were also consistent with those studies. NE might be taken up by myocardial cell via uptake$_2$ carrier and converted to EPI with PNMT. Recent study has shown that gene expression of the PNMT is localized not in cardiac ganglion, but in cardiomyocytes [23]. Therefore, our data suggest that high NE level in myocardial interstitium yields EPI synthesis by regional PNMT activity. NE that was taken up by extraneuronal cells was metabolized mainly to normetanephrine (NMN) or 3-methoxy-4-hydroxyphenylglycol (MHPG) by catechol *O*-methyltransferase (COMT) [19], but high NE was partly available for EPI synthesis with PNMT. These elevated NE levels were similar to the levels of myocardial ischemic regions in our previous studies [6,24]. Therefore, EPI synthesis with PNMT may gain relevance during myocardial ischemia.

4.2. Myocardial interstitial EPI levels during coronary artery occlusion

Coronary occlusion-induced progressive increases in dialysate EPI levels. These increases corresponded to increases in dialysate NE levels. Our data suggest that the high NE level evoked by myocardial ischemia yields EPI synthesis by regional PNMT activity. During myocardial ischemia, calculated ratio of interstitial EPI/NE was eight-times higher than that of NE infusion. In the ischemic heart, normal transport of NE is impaired because of a reduced sodium gradient [5], whereas another uptake system is operative by extraneuronal cells via the uptake$_2$ carrier which is independent of the sodium gradient [25]. Actually myocardial ischemia evoked increases in myocardial interstitial NMN or MHPG via the uptake$_2$ carrier [26]. The time course of dialysate EPI levels corresponded to increases in dialysate NE and NMN levels. Therefore, we consider that released NE is taken up by extraneuronal cells and PNMT activity for EPI synthesis is operative at high concentration of NE.

To confirm EPI synthesis via PNMT activity, we examined ischemia-induced dialysate EPI levels in the presence and absence of a PNMT inhibitor. PNMT inhibition suppressed the increase in dialysate EPI (synthesis by PNMT) and augmented the increase in dialysate NE (substrate of PNMT) levels. Thus, in the ischemic period as well as local administration of NE, PNMT activity plays an important physiological role in NE gradation and EPI synthesis. The PNMT activity in the ischemic left ventricle augmented EPI production by excess of substrate. The increased PNMT activity might reflect compensatory or adaptation processes secondary to impairments of the catecholamine uptake system and its degradation via monoamine oxidase [6].

At the myocardial interstitial space, local ω-conotoxin GVIA treatment attenuated the EPI release in response to cardiac sympathetic nerve stimulation [18]. Furthermore, local tyramine administration caused an increase in dialysate EPI level via a non-exocytotic mechanism. The previous study demonstrated that EPI is released from vesicle and axoplasma via exocytosis and carrier-mediated transport in the cardiac sympathetic nerve endings. In the resting state, myocardial interstitial EPI is extracted mainly from circulating EPI and taken up via catecholamine transporter to nerve endings. Therefore, in the sympathetic nerve endings containing EPI, the non-exocytotic release via outward transport would be involved in EPI release evoked by myocardial ischemia.

Myocardial ischemia-induced increases in dialysate EPI levels were suppressed by the pretreatment with desipramine. Desipramine suppressed peak EPI levels by 5% of vehicle group. Marked suppression of EPI release can be explained by two possible mechanisms. First, desipramine inhibits both directions of NE transport through uptake$_1$ carrier [5,27]. Ischemia-induced outward NE transport through uptake$_1$ carrier is inhibited by desipramine, and so myocardial interstitial NE levels are also attenuated [6]. In this way, desipramine reduced the substrate of EPI via PNMT and EPI synthesis in extraneuronal cells. Alternatively, EPI is released via carrier-mediated outward transport of EPI from sympathetic nerve endings. The present study could not clarify whether EPI specific transporter or NE transporter is involved in carrier-mediated outward transport of EPI. But desipramine inhibits transports of both EPI and NE. Thus, both actions of desipramine on NE and EPI caused a marked decrease in the EPI release evoked by myocardial ischemia. Although desipramine markedly suppressed the EPI release evoked by myocardial ischemia, it is uncertain which factor is more responsible for EPI release.

Finally, to elucidate which of these two mechanisms is mainly involved in the EPI release evoked by myocardial ischemia, we compared ischemia-induced EPI release between desipramine alone and the combination of desipramine and SKF29661 pretreatments. Myocardial ischemia-induced EPI release did not differ between the two groups. This result indicates that the EPI synthesis by PNMT might not be involved in the EPI release evoked by myocardial ischemia. In the presence of desipramine, myocardial interstitial NE levels were markedly suppressed. These NE levels might not be operative as the substrate of EPI whereas only the markedly higher NE level in vehicle group might be operative as the substrate of EPI and yield EPI synthesis via PNMT activity. Thus, PNMT in the left ventricle is capable of synthesizing EPI with markedly elevated NE in the myocardial interstitial space. As well as COMT system [28], cardiac PNMT plays an important physiological role in NE degradation during high concentrations of myocardial interstitial NE. Since EPI preferentially interacts with beta$_2$-adrenergic receptors in heart [29]. Regional EPI might promote exocytotic NE release by activating presynaptic beta$_2$-adrenergic receptors. Future work should concentrate on these aspects of cardiac PNMT.

4.3. Methodological considerations

In general, EPI is released from the adrenal medulla and carried to the heart via the bloodstream [9]. In the present study, we administered a PNMT inhibitor SKF29661 intraperitoneally to block EPI synthesis. SKF29661 may inhibit EPI synthesis at the adrenal grand and reduce blood EPI levels. In this way, administration of SKF29661 might affect EPI uptake and the content of EPI at the cardiac sympathetic nerve endings. There was no significant difference in the control dialysate EPI level between vehicle and SKF29661 group. Therefore, we believe that extraction of EPI from plasma EPI does not change the quantitative results obtained from the cardiac dialysis.

Animal studies demonstrated that two enzymes are involved in EPI synthesis: PNMT and nonspecific *N*-methyltransferase [30]. Nonspecific *N*-methyltransferase is less inhibited by the PNMT inhibitor SKF29661. This nonspecific *N*-methyltransferase was reported to be present in the heart, but the predominant cardiac enzyme is apparently PNMT. Actually pretreatment with SKF29661 suppressed NE-induced EPI release by 10% of vehicle group. Therefore, it is thought that nonspecific *N*-methyltransferase exerts little effect on the EPI release evoked by NE administration or myocardial ischemia.

In conclusion, there is a PNMT activity in the heart. Under local administration of NE or ischemic conditions, PNMT in the left ventricle is capable of synthesizing EPI with markedly elevated NE in the myocardial interstitial space. We consider two mechanisms to be involved in the increment of EPI during myocardial ischemia, namely EPI synthesis by cardiac PNMT in extraneuronal cells and the non-exocytotic release from the sympathetic nerve endings.

Acknowledgements

This work was supported by Grants-in-Aid for scientific research (17591659) from the Ministry of Education, Culture, Sports, Science and Technology. The authors thank Glaxosmithkline for the supply of SKF29661.

References

[1] Lameris TW, de Zeeuw S, Alberts G, Boomsma F, Duncker DJ, Verdouw PD, et al. Time course and mechanism of myocardial catecholamine release during transient ischemia in vivo. Circulation 2000;101:2645–50.

[2] Kuroko Y, Fujii T, Yamazaki T, Akiyama T, Ishino K, Sano S, et al. Contribution of catechol *O*-methyltransferase to the removal of accumulated interstitial catecholamines evoked by myocardial ischemia. Neurosci Lett 2005;388:61–4.

[3] Penny WJ. The deleterious effects of myocardial catecholamines on cellular electrophysiology and arrhythmias during ischaemia and reperfusion. Eur Heart J 1984;5:960–73.

[4] Waldenstrom AP, Hjalmarson AC, Thornell L. A possible role of noradrenaline in the development of myocardial infarction: an experimental study in the isolated rat heart. Am Heart J 1978;95: 43–51.

[5] Schömig A, Dart AM, Dietz R, Mayer E, Kubler W. Release of endogenous catecholamines in the ischemic myocardium of the rat. Part A: locally mediated release. Circ Res 1984;55:689–701.

[6] Akiyama T, Yamazaki T. Myocardial interstitial norepinephrine and dihydroxyphenylglycol levels during ischemia and reperfusion. Cardiovasc Res 2001;49:78–85.

[7] Axelrod J. Purification and properties of phenylethanolamine-*N*-methyl transferase. J Biol Chem 1962;237:1657–60.

[8] Peronnet F, Boudreau G, de Champlain J, Nadeau R. Effect of changes in myocardial epinephrine stores on plasma norepinephrine gradient across the dog heart. Am J Physiol 1994;266:H2404–9.

[9] Elayan HH, Kennedy BP, Ziegler MG. Cardiac atria and ventricles contain different inducible adrenaline synthesising enzymes. Cardiovasc Res 1990;24:53–6.

[10] Ziegler MG, Bao X, Kennedy BP, Joyner A, Enns R. Location, development, control, and function of extraadrenal phenylethanolamine *N*-methyltransferase. Ann N Y Acad Sci 2002;971:76–82.

[11] Akiyama T, Yamazaki T, Ninomiya I. Differential regional responses of myocardial interstitial noradrenaline levels to coronary occlusion. Cardiovasc Res 1993;27:817–22.

[12] Yamazaki T, Akiyama T, Kitagawa H, Takauchi Y, Kawada T, Sunagawa K. A new, concise dialysis approach to assessment of cardiac sympathetic nerve terminal abnormalities. Am J Physiol 1997;272:H1182–7.

[13] Akiyama T, Yamazaki T, Ninomiya I. In vivo monitoring of myocardial interstitial norepinephrine by dialysis technique. Am J Physiol 1991;261: H1643–7.

[14] Yamazaki T, Akiyama T, Shindo T. Routine high-performance liquid chromatographic determination of myocardial interstitial norepinephrine. J Chromatogr B Biomed Appl 1995;670:328–31.

[15] Takauchi Y, Kitagawa H, Kawada T, Akiyama T, Yamazaki T. High-performance liquid chromatographic determination of myocardial interstitial dihydroxyphenylglycol. J Chromatogr B Biomed Sci Appl 1997;693:218–21.

[16] Kennedy B, Elayan H, Ziegler MG. Lung epinephrine synthesis. Am J Physiol 1990;258:L227–31.

[17] Tse J, Rodriques E, Gonzalez M, Weiss HR. Effects of chemical denervation with 6-hydroxydopamine on myocardial responsiveness to isoproterenol in rabbits. Basic Res Cardiol 1995;90:380–7.

[18] Kawada T, Yamazaki T, Akiyama T. Local epinephrine release in the rabbit myocardial interstitium in vivo. J Auton Nerv Syst 2000;78: 94–8.

[19] Trendelenburg U. The extraneuronal uptake and metabolism of catecholamines in the heart. In: Paton DM, editor. The mechanism of neuronal and extraneuronal transport of catecholamines. 1st ed. New York: Raven Press; 1976. p. 259–80.

[20] Grohmann M, Trendelenburg U. The substrate specificity of uptake$_2$ in the rat heart. Naunyn Schmiedebergs Arch Pharmacol 1984;328: 164–73.

[21] Obst OO, Rose H, Kammermeier H. Characterization of catecholamine uptake$_2$ in isolated cardiac myocytes. Mol Cell Biochem 1996;163–164: 181–3.

[22] Torda T, Culman J, Petrikova M. Distribution of phenylethanolamine-*N*-methytransferase in the rat heart: effect of 6-hydroxydopamine. Eur J Pharmacol 1987;141:305–8.

[23] Krizanova O, Micutkova L, Jelokova J, Filipenko M, Sabban E, Kvetnansky R. Existence of cardiac PNMT m-RNA in adult rats: elevation by stress in a glucocorticoid-dependent manner. Am J Physiol Heart Circ Physiol 2001;281:H1372–9.

[24] Shindo T, Akiyama T, Yamazaki T, Ninomiya I. Regional myocardial interstitial norepinephrine kinetics during coronary occlusion and reperfusion. Am J Physiol 1996;270:H245–51.

[25] Schömig E, Russ H, Staudt K, Martel F, Gliese M, Grűndemann. The extraneuronal monoamine transporter exists in human central nervous system glia. Adv Pharmacol 1998;42:356–9.

[26] Fujii T, Yamazaki T, Akiyama T, Sano S, Mori H. Extra neuronal enzymatic degradation of myocardial norepinephrine in the ischemic region. Cardiovasc Res 2004;64:125–31.

[27] Schömig A, Fischer S, Kurz T, Richardt G, Schomig E. Nonexocytotic release of endogenous noradrenaline in during in the ischemic and anoxic rat heart: mechanism and metabolic requirements. Circ Res 1987;60:194–205.
[28] Carlsson L, Graefe KH, Trendelenburg U. Early intraneuronal mobilization and deamination of noradrenaline during global ischemia in the isolated perfused rat heart. Naunyn Schmiedebergs Arch Pharmacol 1987;336:508–18.
[29] Lands AM, Arnold A, McAuliff JP, Luduena FP, Brown Jr TG. Differentiation of receptor systems activated by sympathmimetic amines. Nature 1967;214:597–8.
[30] Zeigler MG, Kennedy B, Elayan H. Extraadrenal adrenaline formation by two separate enzymes. Experintia 1989;45:718–20.

ORIGINAL RESEARCH

Visualization of Intracerebral Arteries by Synchrotron Radiation Microangiography

K. Myojin
A. Taguchi
K. Umetani
K. Fukushima
N. Nishiura
T. Matsuyama
H. Kimura
D.M. Stern
Y. Imai
H. Mori

BACKGROUND AND PURPOSE: Small cerebral vessels are a major site for vascular pathology leading to cerebral infarction and hemorrhage. However, such small cerebral vessels are difficult to visualize by using conventional methods. The goal of our study was the development of methodology allowing visualization of small cerebral arteries in rodents, suitable for experimental models.

MATERIALS AND METHODS: Using barium sulfate as a contrast material, we obtained microangiographic images of physiologic and pathologic changes consequent to cerebral infarction in mouse brain by monochromatic synchrotron radiation (SR). To achieve high-resolution and high-contrast images, we used a new x-ray camera with a pixel size of 4.5 μm, and we set the energy level at 37.5 keV, just above the K absorption of barium.

RESULTS: Small intracerebral arteries (~30 μm in diameter) were clearly visualized, as well as the cortical branches (50–70 μm in diameter) at the brain surface. The limit of detection appeared to be vessels ~10 μm in diameter. Compared with the noninfarcted side, the number of intracerebral arteries was dramatically decreased in the middle cerebral artery area affected by stroke.

CONCLUSIONS: These results indicate the potential of SR for evaluating pathologic changes in small cerebral arteries and for monitoring the impact of pro- and antiangiogenic therapeutic strategies.

Cerebrovascular disease is one of the major causes of death and disability in developed countries. To evaluate cerebral vasculature, conventional angiography and MR angiography are commonly used in clinical practice. The development of these imaging methods has allowed analysis of the pathologic features of cerebrovascular lesions and has guided therapeutic strategies. However, small cerebral vessels, including those known to harbor causative lesions in cerebral infarction and hemorrhage (due to lipohyalinotic changes and/or microaneurysm formation),[1] such as intracerebral arteries and perforators, are below the detection limit of conventional imaging techniques. An important step in developing therapeutic strategies effective against disease in small cerebral vessels is enhanced visualization of this vasculature, especially in experimental models.

Recently, ex vivo and in vivo microangiography using monochromatic synchrotron radiation (SR) has been suggested as a tool capable of visualizing pathophysiologic changes in small arteries. Using this system has made possible the detection of microcirculation in the dermis,[2] tumors,[3] and collateral microvessels in ischemic hind limbs.[4] Although fluorescence microscopy has also been used to image small arteries,[5-7] SR imaging has the advantage of visualizing microvessels, even after they enter the parenchyma of an organ. In contrast, fluorescence techniques do not allow adequate visualization of small arteries once a vessel is deep within brain or other parenchymal tissue. On the basis of these observations, we have developed a microangiographic system using SR and have investigated physiologic and pathologic features of rodent cerebral microvasculature.

Received August 3, 2006; accepted after revision August 31.

From the Departments of Cerebrovascular Disease (K.M., A.T.) and Cardiac Physiology (K.F., N.N., H.M.), National Cardiovascular Center, Osaka, Japan; the Department of Radiology (K.M., Y.I.), Tokai University School of Medicine, Kanagawa, Japan; Japan Synchrotron Radiation Research Institute (K.U.), Hyogo, Japan; the Department of Internal Medicine (T.M.), Hyogo College of Medicine, Hyogo, Japan; Dainippon Sumitomo Pharma Co Ltd (H.K.), Osaka, Japan; and the Dean's Office (D.M.S.), College of Medicine, Cincinnati University, Cincinnati, Ohio.

Experiments were performed at the SPring-8 BL28B2 beamline with the approval of the Japan Synchrotron Radiation Research Institute (acceptance No. 2005B0358).

This work was partially supported by a Grant-in-Aid for Scientific Research from the Ministry of Health, Labor and Welfare and The New Energy and Industrial Technology Development Organization.

Please address correspondence to Akihiko Taguchi, MD, Department of Cerebrovascular Disease, National Cardiovascular Center, 5-7-1 Fujishiro-dai, Suita, Osaka, Japan, 565-8565; e-mail: Taguchi ataguchi@res.ncvc.go.jp

Materials and Methods

All procedures were performed in accordance with the National Cardiovascular Center Animal Care and Use Committee.

Preparation of Contrast Medium

For high-contrast images of the microcirculation, contrast agents included microspheres (Techpolymer I-2, Sekisui Plastics, Shiga, Japan) and barium sulfate (BarytgenSol, Fushimi, Tokushima, Japan). However, because the diameter of microspheres was 15 μm, whereas that of barium sulfate particles varied from 1–100 μm, the microcirculation of cerebral arteries could not be visualized by using these contrast media (not shown). To perfuse such microvessels (diameter <10 μm), we filtered barium sulfate (pore size 5 μm; Millex-SV, Millipore, Bedford, Mass) and obtained particles <5 μm in diameter. Filtered barium sulfate particles were then centrifuged (3000 G, 60 minutes) and concentrated to 50% by weight following removal of the supernatant.

Injection of Contrast Medium

Male severe combined immunodeficient (SCID) mice (6 weeks old; weight, 25–30 g; Oriental Yeast, Tokyo, Japan) were anesthetized by using inhaled diethyl ether and were perfused systemically with phosphate-buffered saline (PBS) containing heparin (40 U/mL) via the left ventricle of the heart with a peristaltic pump (Iwaki, Asahi Techno Glass, Chiba, Japan). Filtered barium sulfate particles (<5 μm in diameter, prepared as described previously; 50% by weight) were infused (0.7 mL), followed by isolation of the brain and fixation in formalin.

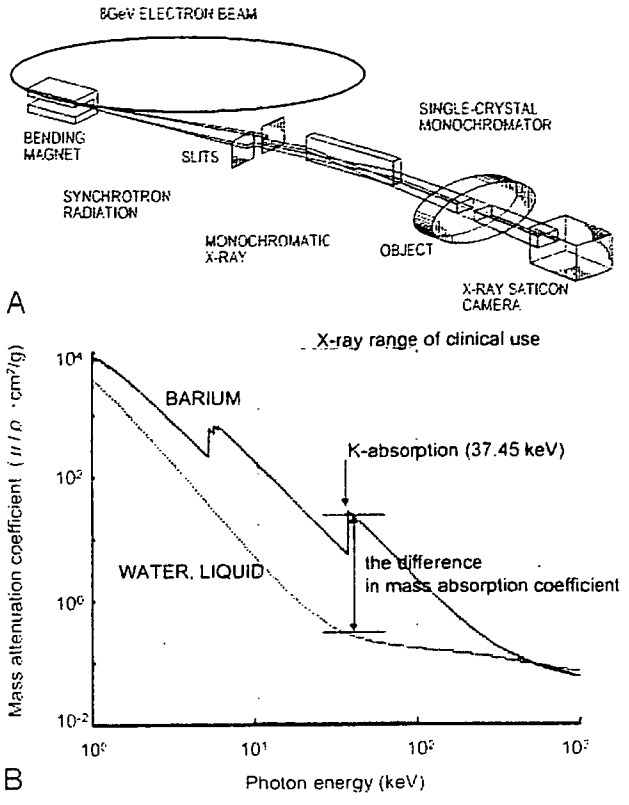

Fig 1. Schematic depiction of the monochromatic SR system. *A*, Illustration of the experimental arrangement for SR microangiography at BL28B2. *B*, Photon mass attenuation coefficient of barium (*blue line*) and liquid water (*red line*). Monochromatic x-ray energy is adjusted to 37.5 keV, just above the barium K-edge energy to produce the highest contrast image.

Microangiography and Image Analysis

Microangiographic images of mouse brain were obtained by using monochromatic SR in the Japan Synchrotron Radiation Research Institute (SPring-8, Hyogo, Japan).[4,8] There are 3 large 3rd-generation synchrotron radiation facilities in the world: the Advanced Photon Source in Argonne (United States), the European Synchrotron Radiation Facility in Grenoble (France), and SPring-8 (the latter was used for the studies described herein). These facilities are open to scientists in many fields, including material, chemical, and life sciences investigators. The experimental setup for x-ray imaging by using monochromatic SR at the SPring-8 BL28B2 beamline is shown in Fig 1*A*. The storage ring was operated at 8-GeV electron beam energy, and beam current was 80–100 mA. The distance between the point source in the bending magnet and the detector was ~45 m. A nearly parallel x-ray beam was used for imaging without blurring because of the small size of the x-ray source and the very long source-to-object distance. The single crystal monochromator selects a single energy of synchrotron radiation. The shutter system is located between the monochromator and the object. X-rays transmitted through the object are detected by an x-ray direct-conversion-type detector incorporating the x-ray saticon pickup tube. Monochromatic x-ray energy was adjusted to 37.5 keV, just above the barium K-edge energy, to produce the highest contrast image of the barium (Fig 1*B*). X-ray flux at the object position was around 1×10^{10} photons/mm^2 per second in imaging experiments. The images were acquired as 1024 × 1024 pixels with 10-bit resolution after analog-to-digital conversion. The FOV was 4.5 × 4.5 mm^2, and pixel size was ~4.5 μm.[9,10]

Mammographic Images

To compare spatial and contrast resolution, we obtained mammographic images, which are known for having the highest resolution in clinical applications,[11] of murine brains. Digital images were captured at an energy level of 24 kV by using a molybdenum target and a molybdenum filter with 90° cranial projection. Source-to-image distance was 65 cm.

Induction of Focal Cerebral Ischemia

Permanent focal cerebral infarction was induced by ligation and disconnection of the left MCA of male SCID mice (n = 5), as described.[12-14] Briefly, under inhaled halothane (3%) anesthesia, animals were placed on their right sides and a skin incision was made at the midpoint between the left orbit and the external auditory canal. The temporalis muscle was incised, and the zygomatic arch was removed to expose the squamous portion of the temporal bone. Using a dental drill, we made a small hole above the distal portion, M1, of the MCA, which could be seen through the exposure in the skull. The dura mater was opened, and the left MCA was electrocauterized and disconnected just distal to its crossing of the olfactory tract. Body temperature was maintained at 36.5°–37°C by using a heat lamp during the operation and for 2 hours after MCA occlusion. Cerebral blood flow (CBF) in the left MCA area was measured by laser-Doppler flowmetry (Advance, Tokyo, Japan). The holding device of the laser probe (ALF probe; Neuroscience, Osaka, Japan) (1.5 mm in diameter, 7.0 mm in length) was secured on the cranium at a site located above the ischemic core of the left MCA area (approximately 1 mm anterior and 5 mm distal to the bregma), and CBF was monitored during the procedure and 24 hours after ligation of the MCA. Mice displaying a decrease in CBF by ~75% immediately after the procedure and thereafter for an additional 24 hours were used for experiments.[15] Nine days after induction of cerebral ischemia, the cerebral microcirculation was examined by SR imaging.

MR Imaging System

To confirm cerebral infarction consequent to ligation of the MCA, we performed MR imaging on day 2 poststroke. MR imaging used a 2T compact MR imaging system with a permanent magnet (MRmini SA206, Dainippon Sumitomo Pharma, Osaka, Japan) by using a radio-frequency solenoid coil for signal-intensity detection. For each imaging sequence, 15 coronal images were acquired with a section thickness of 1 mm, gapped at 0.5 mm. T1-weighted spin-echo MR images were acquired with a TR/TE of 500/9 ms, a FOV of 36.6 × 18.3 mm, an image acquisition matrix of 256 × 128, and NEX, 4. T2-weighted spin-echo MR images were obtained with TR/TE, 3000/69, 256 × 128, and NEX, 2. Because the sequences to obtain diffusion-weighted images by using this machine are still in development, we evaluated the cerebral ischemia by T2-weighted images on day 2 poststroke.

Data Analysis

In all experiments, the mean ± SE is reported.

Results

Visualization of Cerebral Arteries by SR Imaging

After euthanasia and systemic perfusion with PBS, barium sulfate particles were infused via the left ventricle of the heart. As shown in Fig 2*A*, cerebral arteries on the brain surface were filled with contrast medium. First, we investigated vascular

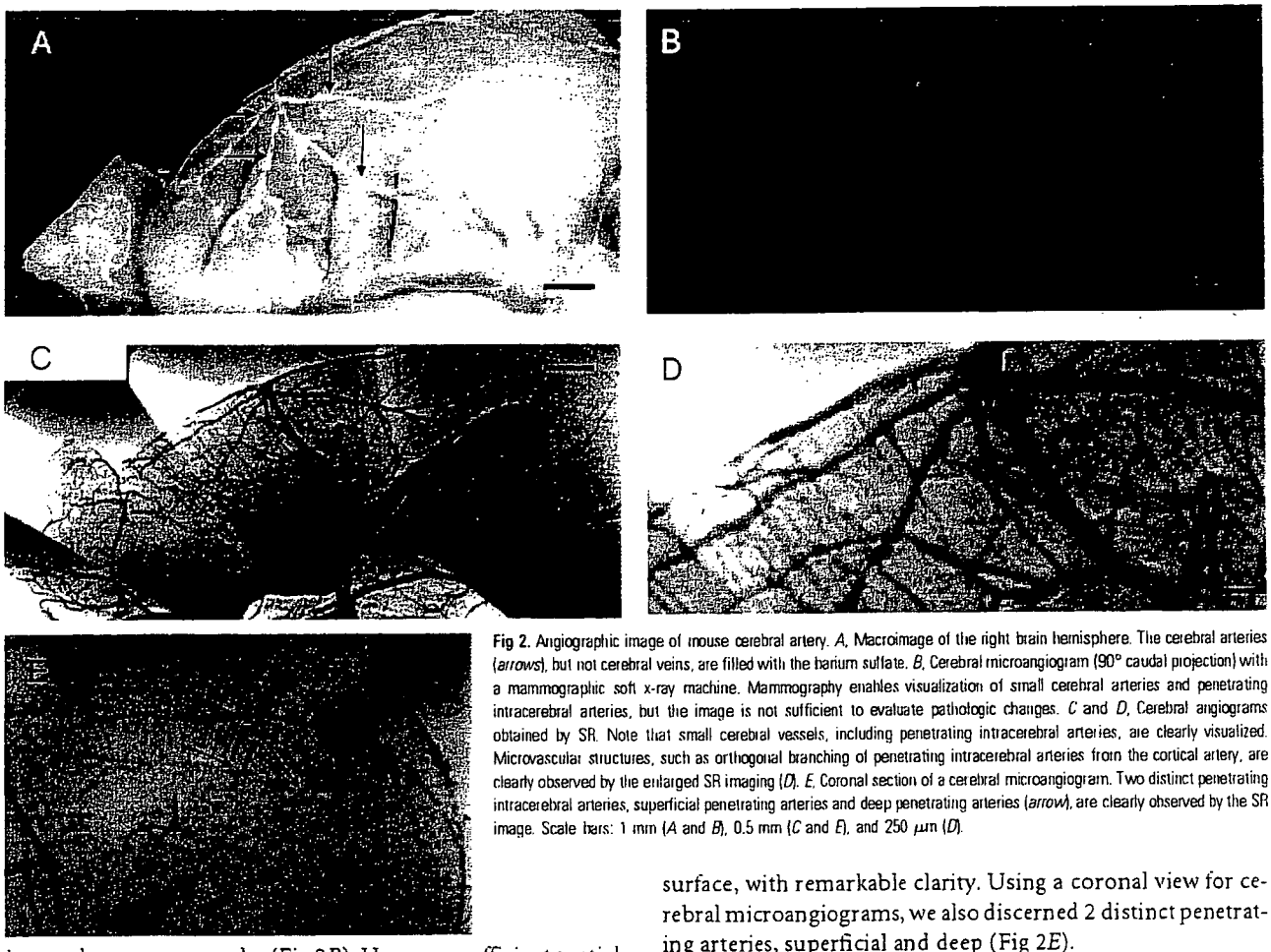

Fig 2. Angiographic image of mouse cerebral artery. *A*, Macroimage of the right brain hemisphere. The cerebral arteries (*arrows*), but not cerebral veins, are filled with the barium sulfate. *B*, Cerebral microangiogram (90° caudal projection) with a mammographic soft x-ray machine. Mammography enables visualization of small cerebral arteries and penetrating intracerebral arteries, but the image is not sufficient to evaluate pathologic changes. *C* and *D*, Cerebral angiograms obtained by SR. Note that small cerebral vessels, including penetrating intracerebral arteries, are clearly visualized. Microvascular structures, such as orthogonal branching of penetrating intracerebral arteries from the cortical artery, are clearly observed by the enlarged SR imaging (*D*). *E*, Coronal section of a cerebral microangiogram. Two distinct penetrating intracerebral arteries, superficial penetrating arteries and deep penetrating arteries (*arrow*), are clearly observed by the SR image. Scale bars: 1 mm (*A* and *B*), 0.5 mm (*C* and *E*), and 250 μm (*D*).

images by mammography (Fig 2*B*). However, sufficient spatial and contrast resolution was not obtained by mammographic imaging to evaluate the angioarchitecture of small cerebral vasculature. Peripheral branches of the MCA (75–100 μm in diameter) and small vessels emerging from peripheral branches were barely visualized.

Next, we investigated the vascular profile by using SR (Fig 2*C*, normal view; -*D*, enlarged view). At the brain surface, cortical arteries branching from the MCA and pial arteries, ~30 μm in diameter, were clearly visualized. Within the brain parenchyma, penetrating intracerebral arteries, branching orthogonally from cortical or pial arteries, were also observed. The interval between intracerebral arteries was 126.1 ± 35.5 μm (n = 20), the diameter of the proximal side of the intracerebral arteries was 29.5 ± 3.1 μm (n = 20), and each intracerebral artery was observed to progressively narrow to a diameter below the limit of resolution (10 μm). Vascular diameters determined by SR imaging of intracerebral arteries and small arterial branches were identical to those observed in previous pathologic studies of murine brain.[16] Using SR imaging, we could discern 2 types of intracerebral arteries: superficial penetrating arteries perfusing only the cortical area and penetrating arteries reaching the subcortical area and perfusing the deep white matter. These vascular structures observed in murine brain by SR imaging are similar to previous observations in human anatomic studies.[17-20] Compared with mammographic images, SR imaging enabled visualization of penetrating intracerebral arteries (diameter range of 10–30 μm), as well as small peripheral branches of MCA at the brain surface, with remarkable clarity. Using a coronal view for cerebral microangiograms, we also discerned 2 distinct penetrating arteries, superficial and deep (Fig 2*E*).

SR Images after Cerebral Infarction

To evaluate cerebral vasculature in the context of pathologic changes, cerebral infarction was induced by ligation of the MCA. The area of cerebral infarction was visualized by MR imaging on day 2 after induction of stroke. As we have shown previously by 2,3,5-triphenyltetrazolium staining,[12] limited cortical infarction was observed in the MCA area on T2-weighted images (Fig 3*A*). In contrast, no hyper- or hypointense region was observed on T1-weighted images (Fig 3*B*), indicating the absence of bleeding or parenchymal injury. Although no morphologic (Fig 3*C*) or vascular structural (Fig 3*D*) changes were observed in the right hemisphere (nonstroke side), by day 9 after MCA occlusion, tissue degradative changes were observed in the cortical and shallow white matter of the left MCA area (stroke side, Fig 3*E*). To evaluate the integrity of the microvasculature after stroke, we obtained SR images. The number of penetrating intracerebral arteries dramatically decreased, though cortical branches at the brain surface could still be visualized (Fig 3*F*). On the coronal view, the disappearance of the intracerebral arteries on the ischemic side was also clearly observed (Fig 3*G*).

Discussion

Cerebral artery disease in small vessels is a major cause of cerebral infarction and hemorrhage. Although pathologic changes in small arteries have been reported on the basis of microscopic analysis, it has been difficult to assess the mor-

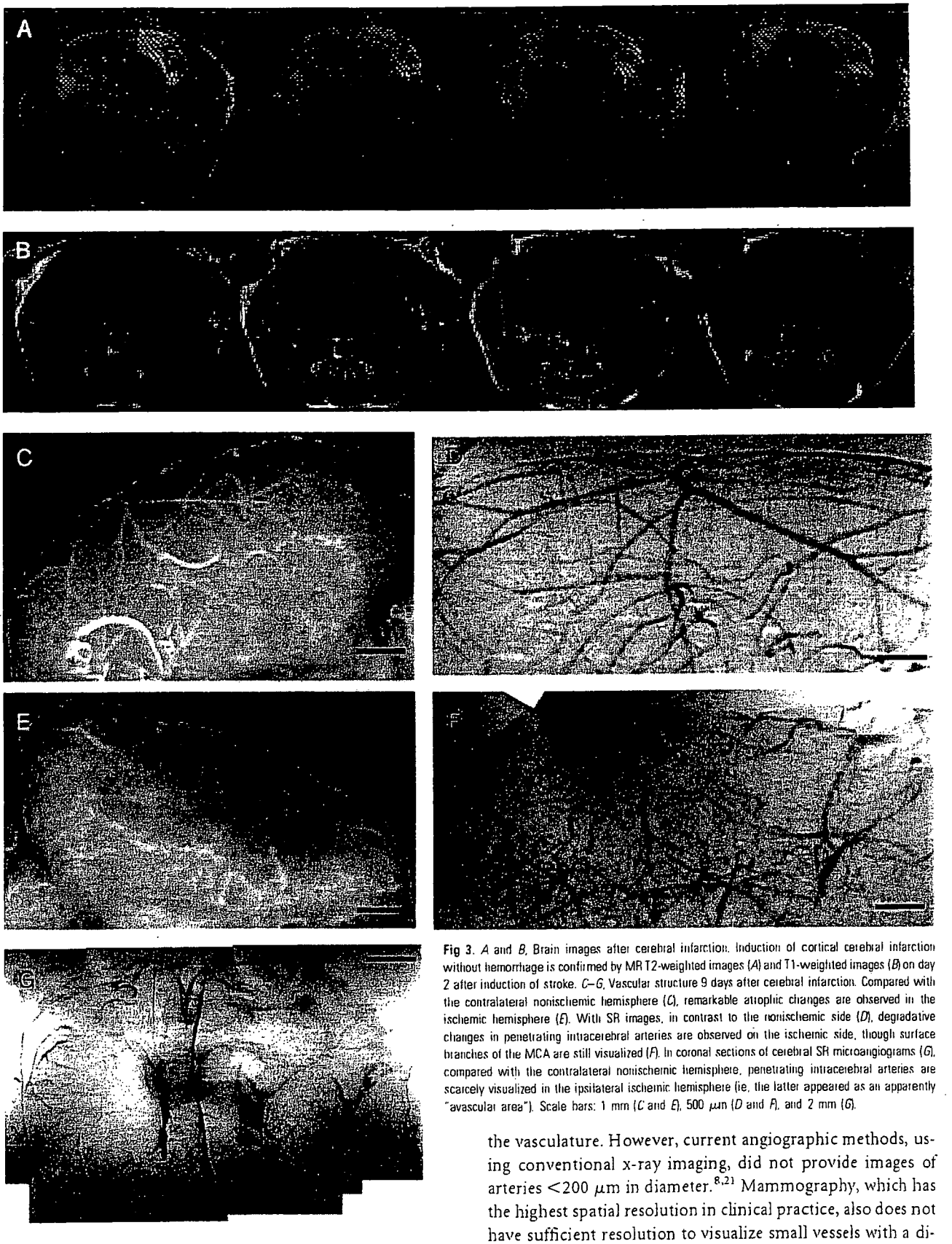

Fig 3. *A* and *B*, Brain images after cerebral infarction. Induction of cortical cerebral infarction without hemorrhage is confirmed by MR T2-weighted images (*A*) and T1-weighted images (*B*) on day 2 after induction of stroke. *C–G*, Vascular structure 9 days after cerebral infarction. Compared with the contralateral nonischemic hemisphere (*C*), remarkable atrophic changes are observed in the ischemic hemisphere (*E*). With SR images, in contrast to the nonischemic side (*D*), degradative changes in penetrating intracerebral arteries are observed on the ischemic side, though surface branches of the MCA are still visualized (*F*). In coronal sections of cerebral SR microangiograms (*G*), compared with the contralateral nonischemic hemisphere, penetrating intracerebral arteries are scarcely visualized in the ipsilateral ischemic hemisphere (ie, the latter appeared as an apparently "avascular area"). Scale bars: 1 mm (*C* and *E*), 500 μm (*D* and *F*), and 2 mm (*G*).

phology of small cerebral vessels in situ through imaging studies. Herein, we demonstrate that small cerebral vessels can be clearly visualized by microangiography by using SR.

Conventional angiography is commonly used to evaluate the vasculature. However, current angiographic methods, using conventional x-ray imaging, did not provide images of arteries <200 μm in diameter.[8,21] Mammography, which has the highest spatial resolution in clinical practice, also does not have sufficient resolution to visualize small vessels with a diameter of <50 μm.[11] Microangiographic techniques have been developed by using fine-focus x-rays and sensitive films to evaluate the microcirculation in the brain.[20] These methods enable visualization of human cortical perforating arteries and

medullary long branches (100 μm in diameter) by using 1-cm-thick sections of brain.[20] However, the limit of detection by using these methods applied to thick sections has been reported to be vessels of 50 μm in diameter.[22] Furthermore, visualization of smaller arteries required thin sections cut with a microtome.[20] The latter method is not well-suited to the evaluation of 3D cerebral vascular trees.

Compared with these conventional methods, the principal advantage of SR is the small size of the electron beam, thereby providing a high-intensity x-ray point source. Using a nearly parallel beam of SR, along with a precise detection system (pixel size of 4.5 μm), allowed us to obtain high-quality angiographic images with excellent spatial resolution. Furthermore, setting SR at an energy level just above the K absorption of barium produced the highest contrast images. SR imaging provides a powerful tool to reveal the morphology of small cerebral arteries such as superficial and deep penetrating arteries, allowing analysis of their physiologic and pathologic properties under a variety of conditions (ie, borderzone in infarction[23,24] and microaneurysm formation).

Fluorescence microscopy is another tool potentially useful for analysis of the microcirculation.[25] Although fluorescence microscopy provides visualization of microcirculation at the brain surface, the advantage of SR imaging is visualization of small vessels that have penetrated into the brain parenchyma, such as the subcortex. In addition, SR imaging allows performance of microangiography with an optimal projection. When the latter is combined with a microinjector, sequential real-time images can be obtained, providing the substrate for hemodynamic analysis.

In this article, we investigated SR imaging after stroke and showed that the SR image reflects pathologic changes previously observed by using anatomic/microscopic analysis. On day 9 after MCA occlusion, arteries on the surface of the cerebrum were visualized by SR, though penetrating intracerebral arteries were not detected. Previous studies have shown that the integrity of the distal cortical artery is usually maintained after occlusion of the proximal artery and that collateral flow is established through expansion of previously existing and/or formation of new vascular channels.[25,26] Analysis with enhanced MR imaging has shown cerebral parenchymal enhancement in the stroke area by 1 week after cerebral infarction,[27] indicative of blood flow in the peri-ischemic area. In contrast, penetrating intracerebral arteries were dramatically decreased in number in the ischemic hemisphere, though cortical branches on the brain surface were maintained after MCA occlusion. It has previously been shown that microvasculature in the ischemic territory displays adhesion of polymorphonuclear leukocytes in postcapillary venules, followed by the disruption of the microvascular network.[28] These previous findings are consistent with the results of our vascular images obtained by SR after ligation of the MCA.

Conclusion

Our study demonstrates, for the first time, the morphologic features of small vascular networks in murine brain by microangiography by using SR imaging. Our approach provides a powerful tool for evaluating potential angiogenic/antiangiogenic therapeutic strategies, as well as pathologic examination of the cerebral microarterial tree.

Acknowledgments

We thank Y. Kasahara, K. Tomiyasu, and M. Aoki for technical assistance.

References

1. Phillips SJ, Whisnant JP. **Hypertension and the brain: The National High Blood Pressure Education Program.** *Arch Intern Med* 1992;152:938–45
2. Ito K, Tanaka E, Mori H, et al. **A microangiographic technique using synchrotron radiation to visualize dermal circulation in vivo.** *Plast Reconstr Surg* 1998;102:1128–33
3. Tokiya R, Umetani K, Imai S, et al. **Observation of microvasculatures in athymic nude rat transplanted tumor using synchrotron radiation microangiography system.** *Academic Radiology* 2004;9:1039–46
4. Takeshita S, Isshiki T, Mori H, et al. **Use of synchrotron radiation microangiography to assess development of small collateral arteries in a rat model of hindlimb ischemia.** *Circulation* 1997;95:805–08
5. Conway JG, Popp JA, Thurman RG. **Microcirculation in periportal and pericentral regions of lobule in perfused rat liver.** *Am J Physiol* 1985;249:G449–56
6. Stock RJ, Cilento EV, McCuskey RS. **A quantitative study of fluorescein isothiocyanate-dextran transport in the microcirculation of the isolated perfused rat liver.** *Hepatology* 1989;9:75–82
7. Birngruber R, Schmidt-Erfurth U, Teschner S, et al. **Confocal laser scanning fluorescence topography: a new method for three-dimensional functional imaging of vascular structures.** *Graefes Arch Clin Exp Ophthalmol* 2000;238:559–65
8. Mori H, Hyodo K, Tanaka E, et al. **Small-vessel radiography in situ with monochromatic synchrotron radiation.** *Radiology* 1996;201:173–77
9. Umetani K, Yagi N, Suzuki Y, et al. **Observation and analysis of microcirculation using high-spatial-resolution image detectors and synchrotron radiation.** *Proceeding of SPIE* 2000;3977:522–33
10. Yamashita T, Kawashima S, Ozaki M, et al. **Images in cardiovascular medicine: mouse coronary angiograph using synchrotron radiation microangiography.** *Circulation* 2002;105:E3–4
11. Kuzmiak CM, Pisano ED, Cole EB, et al. **Comparison of full-field digital mammography to screen-film mammography with respect to contrast and spatial resolution in tissue equivalent breast phantoms.** *Med Phys* 2005;32:3144–50
12. Taguchi A, Soma T, Tanaka H, et al. **Administration of CD34+ cells after stroke enhances neurogenesis via angiogenesis in a mouse model.** *J Clin Invest* 2004;114:330–38
13. Furuya K, Kawahara N, Kawai K, et al. **Proximal occlusion of the middle cerebral artery in C57Black6 mice: relationship of patency of the posterior communicating artery, infarct evolution, and animal survival.** *J Neurosurg* 2004;100:97–105
14. Kitagawa K, Matsumoto M, Mabuchi T, et al. **Deficiency of intercellular adhesion molecule 1 attenuates microcirculatory disturbance and infarction size in focal cerebral ischemia.** *J Cereb Blood Flow Metab* 1998;18:1336–45
15. Matsushita K, Matsuyama T, Nishimura H, et al. **Marked, sustained expression of a novel 150-kDa oxygen-regulated stress protein, in severely ischemic mouse neurons.** *Brain Res Mol Brain Res* 1998;60:98–106
16. Coyne EF, Ngai AC, Meno JR, et al. **Methods for isolation and characterization of intracerebral arterioles in the C57/BL6 wild-type mouse.** *J Neurosci Methods* 2002;120:145–53
17. Herman LH, Ostrowski AZ, Gurdjian ES. **Perforating branches of the middle cerebral artery: an anatomical study.** *Arch Neurol* 1963;8:32–34
18. Kaplan HA. **The lateral perforating branches of the anterior and middle cerebral arteries.** *J Neurosurg* 1965;23:305–10
19. de Reuck J. **The area of the deep perforating branches of the median cerebral artery in man [in French].** *Acta Anat (Basel)* 1969;74:30–35
20. Salamon G, Combalbert A, Faure J, et al. **Microradiographic study of the arterial circulation of the brain.** *Prog Brain Res* 1968;30:33–41
21. Mori H, Hyodo K, Tobita K, et al. **Visualization of penetrating transmural arteries in situ by monochromatic synchrotron radiation.** *Circulation* 1994;89:863–71
22. Salamon G, Raybaud C, Michotey P, et al. **Angiographic study of cerebral convolutions and their area of vascularization [in French].** *Rev Neurol (Paris)* 1975;131:259–84
23. Bogousslavsky J, Regli F. **Centrum ovale infarcts: subcortical infarction in the superficial territory of the middle cerebral artery.** *Neurology* 1992;42:1992–98
24. Donnan GA, Norrving B, Bamford JM, et al. **Subcortical infarctions: classification and terminology.** *Cerebrovasc Dis* 1993;3:248–51
25. Tomita Y, Kubis N, Calando Y, et al. **Long-term in vivo investigation of mouse cerebral microcirculation by fluorescence confocal microscopy in the area of focal ischemia.** *J Cereb Blood Flow Metab* 2005;25:858–67
26. Zulch KJ. *Cerebral Circulation and Stroke.* Berlin, Germany: Springer-Verlag; 1971:116
27. Merten CL, Knitelius HO, Assheuer J, et al. **MRI of acute cerebral infarcts: increased contrast enhancement with continuous infusion of gadolinium.** *Neuroradiology* 1999;41:242–48
28. del Zoppo GJ, Mabuchi T. **Cerebral microvessel responses to focal ischemia.** *J Cereb Blood Flow Metab* 2003;23:879–94

Intense clean characteristic flash x-ray irradiation from an evaporating molybdenum diode

Michiaki Sagae
Eiichi Sato, MEMBER SPIE
Iwate Medical University
Department of Physics
3-16-1 Honchodori
Morioka 020-0015, Japan
E-mail: msagae@iwate-med.ac.jp

Etsuro Tanaka
Tokyo University of Agriculture
Department of Nutritional Science
Faculty of Applied Bioscience
1-1-1 Sakuragaoka
Setagaya-ku 156-8502, Japan

Hidezo Mori
National Cardiovascular Center Research Institute
Department of Cardiac Physiology
5-7-1 Fujishirodai, Suita
Osaka 565-8565, Japan

Toshiaki Kawai, MEMBER SPIE
Hamamatsu Photonics K. K.
Electron Tube Division 2
314-5 Shimokanzo
Iwata 438-0193, Japan

Takashi Inoue
Akira Ogawa
Iwate Medical University
Department of Neurosurgery
School of Medicine
19-1 Uchimaru
Morioka 020-8505, Japan

Shigehiro Sato
Iwate Medical University
Department of Microbiology
School of Medicine
19-1 Uchimaru
Morioka 020-8505, Japan

Kazuyoshi Takayama, MEMBER SPIE
Tohoku University
Shock Wave Research Center
Institute of Fluid Science
2-1-1 Katahira
Sendai 980-8577, Japan

Jun Onagawa
Hideaki Ido
Tohoku Gakuin University
Department of Applied Physics and Informatics
Faculty of Engineering
1-13-1 Chuo
Tagajo 985-8537, Japan

Abstract. In a flash x-ray generator, a 150-nF condenser is charged up to 80 kV by a power supply, and flash x-rays are produced by the discharge. The x-ray tube is a demountable diode, and the turbomolecular pump evacuates air from the tube with a pressure of approximately 1 mPa. Since the electric circuit of the high-voltage pulse generator employs a cable transmission line, the high-voltage pulse generator produces twice the potential of the condenser charging voltage. Because bremsstrahlung rays are not emitted in the opposite direction of that of electron trajectory, clean molybdenum K-series characteristic x-rays can be produced without using a filter. When the charging voltage is increased, the K-series characteristic x-ray intensities of molybdenum increase. The K lines are clean and intense, and hardly any bremsstrahlung rays are detected. The x-ray pulse widths are approximately 100 ns, and the time-integrated x-ray intensity has a value of approximately 500 μGy per pulse at 1.0 m from the x-ray source, with a charging voltage of 80 kV.
[DOI: 10.1117/1.2541668]

Subject terms: flash x-ray; energy-selective radiography; characteristic x-rays; quasi-monochromatic x-rays; bremsstrahlung x-ray distribution.

Paper 050104R received Feb. 7, 2005; revised manuscript received Jan. 10, 2006; accepted for publication Aug. 10, 2006; published online Mar. 2, 2007. This paper is a revision of a paper presented at the SPIE conference on 26th International Congress on High-Speed Photography and Photonics, Sep. 2004, Alexandria, Virginia. The paper presented there appears (unrefereed) in SPIE proceedings Vol. 5580.

1 Introduction

In recent years, there have been several investigations dealing with the production of monochromatic x-rays in radiology and cardiology. Particularly, monochromatic parallel beams using synchrotrons have been employed to perform enhanced K-edge angiography[1,2] and x-ray phase imaging.[3,4] In angiography, parallel beams with photon energies of approximately 35 keV have been employed, since these beams are absorbed effectively by an iodine-based contrast medium. Subsequently, in cases where phase imaging is employed, the spatial resolution can be improved, and the number of tissues that can be observed using x-rays increases.

We have developed several different soft flash x-ray generators[5–11] with photon energy of less than 150 keV corresponding to specific radiographic objectives, and a major goal in our research is the development of an intense and clean monochromatic x-ray generator that can impact applications with medical radiography. Recently, we have succeeded in producing intense K-series characteristic x-rays from the axial direction of linearly evaporating targets.[12–16] In metal vapor, bremsstrahlung spectra with photon energies of higher than the K-absorption edge are effectively absorbed and are converted into fluorescent x-rays. The vapor then transmits the fluorescent rays easily. However, the bremsstrahlung x-rays are produced using a molybdenum target,[12] since high-photon-energy bremsstrahlung x-rays are not absorbed effectively in the linear vapor.

To produce clean characteristic x-rays of molybdenum, silver, cerium, ytterbium, and tungsten, we have developed a compact and weak flash x-ray generator,[17] and succeeded in producing clean molybdenum K-series characteristic x-rays of approximately 1×10^7 photons/cm^2 at 1.0 m per pulse using the angle dependence of bremsstrahlung x-rays, since bremsstrahlung rays are not emitted in the opposite direction to that of electron trajectory. Therefore, the K photons should be maximized by increasing both the tube voltage and current, and monochromatic Kα rays are selected using a zirconium filter.[18] Furthermore, both the bremsstrahlung and characteristic x-rays are produced in a metal vapor, and the vapor transmits K-series characteristic x-rays easily. Thus, we are very interested in the x-ray characteristics of a diode with an evaporating target formed by increasing the electrostatic energy in a high-voltage condenser.

In this work, we developed a new flash x-ray generator utilizing a ring-cathode molybdenum diode, used to perform a preliminary experiment for generating intense and clean K-series characteristic x-rays from an evaporated molybdenum target tip utilizing the angular dependence of the bremsstrahlung x-ray distribution.

2 Generator

2.1 *High-Voltage Circuit*

Figure 1 shows a block diagram of an intense flash x-ray generator. The generator consists of the following essential components: a high-voltage power supply, a high-voltage condenser with a capacity of approximately 150 nF, an air gap switch, a turbomolecular pump, a thyratron pulse generator as a trigger device, and a flash x-ray tube. In this generator, a four-cable transmission line is employed to increase maximum tube voltage using high-voltage reflection and to decrease the impedance of the generator. The high-voltage main condenser is charged up to 80 kV by the power supply, and electric charges in the condenser are discharged to the tube through the four cables after closing the gap switch with the trigger device (Fig. 2).

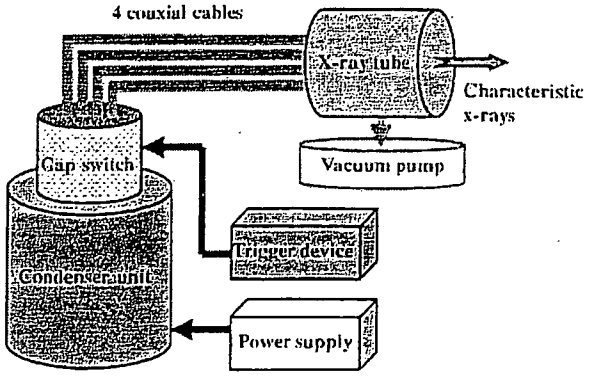

Fig. 1 Block diagram of the intense characteristic flash x-ray generator with a ring-cathode molybdenum diode.

2.2 *X-Ray Tube*

The x-ray tube is a demountable cold-cathode diode that is connected to the turbomolecular pump with a pressure of approximately 1 mPa (Fig. 3). This tube consists of the following major parts: a ring-shaped graphite cathode with an inside diameter of 4.5 mm, a stainless-steel vacuum chamber, a nylon insulator, a polyethylene terephthalate (Mylar) x-ray window 0.25 mm in thickness, and a rod-shaped molybdenum target 3.0 mm in diameter. The distance between the target and cathode electrodes can be regulated from the outside of the tube, and is set to 1.5 mm. As electron beams from the cathode electrode are roughly converged to the target by the electric field in the tube, the vapor x-ray source forms at the solid target tip. Because bremsstrahlung rays are not emitted in the opposite direction to that of the electron trajectory (Fig. 4), clean molybdenum K-series characteristic x-rays can be produced without using a molybdenum filter.

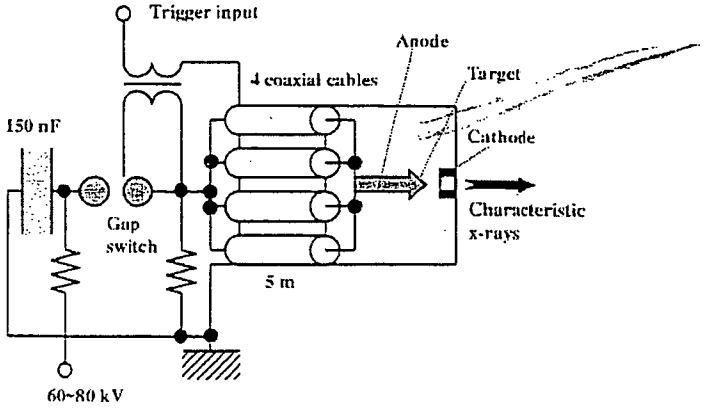

Fig. 2 Circuit diagram of the flash x-ray generator utilizing a coaxial transmission line.